Research article

Adsorption of neutral red dye by chitosan and activated carbon composite films

Fabiana Paiva de Freitas [*], Ana Márcia Macedo Ladeira Carvalho,
Angélica de Cássia Oliveira Carneiro, Mateus Alves de Magalhães, Mariana Fonseca Xisto,
Wagner Davel Canal

Universidade Federal de Viçosa, Brazil

ABSTRACT

Research indicates the use of adsorbent materials to remove pollutants from wastewater and effluents, which can be obtained from renewable materials such as biomass, biopolymers (chitosan) or composites. Thus, the objective of this work was to produce and evaluate activated carbon (AC) and chitosan composite films as adsorbents of neutral red dye. AC films were produced using CO_2 and water vapor. The variables of the activation process were time (1 and 2 h) and temperature (600 and 750 °C). Five films were produced, with one pure chitosan (T1) film and four activated carbon with chitosan films (T2, T3, T4 and T5). The T2 film refers to activated carbon produced at 600 °C for 1 h + chitosan, T3 to activated carbon produced at 600 °C for 2 h + chitosan, T4 to activated carbon produced at 750 °C for 1 h + chitosan and T5 to activated carbon produced at 750 °C for 2 h + chitosan. The T5 film increased its adsorption capacity by approximately 87% and its removal efficiency of neutral red dye by 43% compared to T1. The presence of activated carbon in the films provided an increase in the adsorption capacity of the neutral red dye.

1. Introduction

Dyes and pigments are widely used mainly in textile, paper, plastics, leather, food and cosmetics industries to give color to their products. Their release into effluents can pose a great risk to the environment and human health because the dyes are visible and carcinogenic even in small quantities. As a result, governments establish environmental policies and restrictions on wastewater quality, and industries are required to exercise effluent treatment (Gupta et al., 2013). Most dyes are toxic, including neutral red, which is a cationic dye widely used in biological research to dye embryonic tissues and living cells. Neutral red can produce carbon monoxide, carbon dioxide, nitrogen oxides and hydrogen chlorides which are harmful to human health (Iram et al., 2010).

Research points to the use of a wide variety of adsorbent materials to remove pollutants from water resources, which can be obtained from renewable materials such as biomass or biopolymers; for example, by corn stalk powder and chitosan (Rahmi and Rizki, 2018).

Chitosan is a biopolymer synthesized from the deacetylation of chitin. It is found in crustacean shellfish (crab, shrimp, lobster), and also in the cell wall of fungi, being one of the most abundant biopolymers in nature (Liu et al., 2012). Chitosan has amine and hydroxyl groups in its composition, which make its structure chemically reactive (Karaer and Kaya, 2016) and its versatility is attributed to free amine groups which are exposed after chitin deacetylation reactions, increasing the amount of active sites and providing selectivity in the adsorption process (Zhang et al., 2016). However, this pure biopolymer used as an adsorbent has some disadvantages such as low chemical stability and mechanical resistance. Nevertheless, these characteristics can be optimized by adding a crosslinking and loading agent during the usage process (Tran et al., 2013).

In addition, studies indicate that the spherical or film shape of chitosan particles results in increased surface area and becomes a favorable characteristic for adsorbing pollutants, different from commercial chitosan, which has the appearance of geometrically irregular particles (Andrade et al., 2012; Carvalho et al., 2019).

---

* Corresponding author.
E-mail address: fabianapf@hotmail.com (F.P. de Freitas).

Substances are added as support for chitosan's immobilization to improve its performance as an adsorbent, such as sand, clay and activated carbon. The use of activated carbon as a support has advantages because it is a material with good adsorption capacity for different types of pollutants, it has a high surface area, and good mechanical and chemical resistance (Sharififard et al., 2016).

Due to its cost and physical chemical properties, biochar or activated carbon has proven to be a promising adsorbent for various contaminants, including metals, anions, aromatics, hydrocarbons, and polychlorinated compounds. In addition, biochar offers other advantages such as improving soil quality, reducing greenhouse gas emissions, and acting as green building materials and green catalysts for sustainable biorefinery. It can also be used in cosmetics and personal care products such as toothpaste (Kumar et al., 2020).

Thus, the objective of the work was to produce chitosan and activated carbon composite films physically derived from forest biomass, as well as to evaluate the maximum adsorption capacity and adsorption kinetics of the neutral red dye by the composite films.

2. Material and methods

2.1. Collection and preparation of ACs precursor material

Pinus spp. plywood panel residue from the joinery of the Forestry Engineering Department of the Federal University of Viçosa was used as precursor material. The material was fragmented in a hammer mill, sieved and selected through the 40 mesh sieve and retained in the 60 mesh sieve.

2.2. Characterization of precursor materials

2.2.1. Chemical composition

The elemental chemical composition (carbon, nitrogen, hydrogen and sulfur) of the residue and chitosan were determined according to DIN EN 15104 (Deutsches Institut für Normung, 2011a). The ash content was determined according to the standard of ABNT NBR 8112 (ABNT, 1986) and the oxygen content was determined by the sum of carbon, nitrogen, hydrogen, sulfur and ash content decreased by 100, according to DIN EN 15296 (Deutsches Institut für Normung, 2011b).

2.3. Production of charcoal and activated carbons (ACs)

The stages of the activated carbon production process are represented by the desired grain size adjustment (powder), followed by the carbonization process, and finally the activation stage. The plywood residue carbonization was carried out in a muffle furnace.

First, water vapor produced in an autoclave was used to physically activate charcoal under a pressure of 1.5 kg cm^{-2} at 127 °C and CO_2, with a flow rate of approximately 5.3 g min^{-1} and 120 ml min^{-1}, respectively. A 115 g mass of the carbonized material was subjected to gas action inside a stainless steel reactor, which was inserted into a muffle furnace. The gas and steam were injected by a silicone hose coupled to a pipe running through the reactor cover. The final part of this pipe has 6 perforations which enable homogenization of gases with the material inside the reactor. The temperatures and times used in the physical activation process were 600 and 750 °C and 1 and 2 h, respectively.

2.4. Activated carbon and chitosan composite films

The composite films were prepared by dissolving 4 g of chitosan powder in 100 mL of acetic acid 5 % (m/v). Then, 4 g of powdered activated carbon was added into this solution, remaining under stirring for 1 h until complete homogenization. The formed gel was poured into petri dishes of 10 cm in diameter and dried in oven at 60 °C for 8 h until the solvent evaporated and the films were formed. Next, a solution of NaOH (1 mol.L^{-1}) was added to the films until they were covered, which remained at rest for 24 h, and then washed with deionized water (adapted from Marques Neto et al., 2019). The pure chitosan film was synthesized in the same way, meaning without the addition of activated carbon. Figure 1 shows the synthesis process of AC and chitosan composite films.

A pure chitosan film, represented by T1, and four activated carbon with chitosan films were produced. The T2 film refers to activated carbon produced at 600 °C for 1 h + chitosan, T3 to activated carbon produced at 600 °C for 2 h + chitosan, T4 to activated carbon produced at 750 °C for 1 h + chitosan and T5 to activated carbon produced at 750 °C for 2 h + chitosan.

2.5. Characterization of films

The elemental chemical composition (carbon, nitrogen, hydrogen and oxygen) was determined according to DIN EN 15104 (Deutsches Institut für Normung, 2011a) and the ash content according to ABNT NBR 8112 (ABNT, 1986) using a CHNS analyzer (Vario Micro Cube, Elementar®).

Infrared spectroscopy was used to determine the functional chemical groups. Approximately 2 mg of each film were analyzed in a VARIAN 660 IR instrument with total attenuated reflectance attachment (PIK Glande ATR) in a spectral range of 400–4000 cm^{-1}.

X-ray diffractometry is a technique for characterizing crystal structures. Diffraction is an interference that occurs when a wave encounters an obstacle and it is able to bypass obstacles and disperse. The film analysis was processed in an X-ray diffractometer model D8 Discover
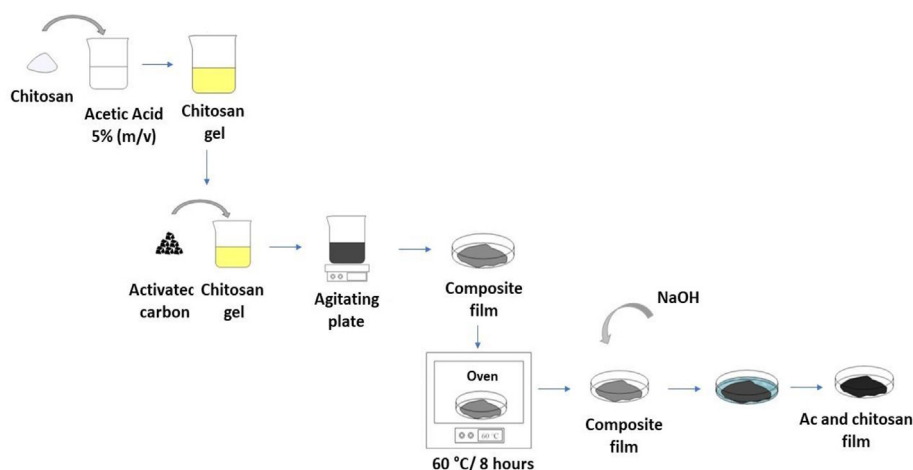
Figure 1. Scheme of the production process of composite films.

(Bruker) using Cu-Kα radiation (λ = 0.1541 nm), with an angular variation 2θ from 10 to 50° and scan rate of 0.05° s^{-1}.

Approximately 10 mg of each film was treated at 150 °C under nitrogen flow for 4 h. The adsorption and desorption isotherms of N$_2$ of the films were performed at 77 K using AUTOSORB-1 equipment (Quantachrome). The specific surface area was calculated using the BET equation and the pore volume and diameter using the BJH method for mesoporous treatment and the HK method for microporous treatment.

Neutral red cationic dye (NR) was used to obtain the adsorption isotherms of the films. First, 0.1 g samples of the films were added in 10 mL of the NR solutions with different concentrations (100, 200, 300, 400 and 500 mg.L^{-1}) for each film. Then these solutions were kept under agitation at 100 rpm in an agitating plate for 24 h at neutral pH and room temperature.

Equilibrium concentrations were measured with a UV-Visible spectrophotometer (Applied Biosystems, UV SP-2000 model). Analytical curves were constructed from the dilution of a stock solution of 2,000 mg.L^{-1} with a concentration range of 1.00 mg.L^{-1} at 20.00 mg.L^{-1}. Aliquots of 100 μL were taken at pre-established intervals for each vial containing AM and NR and equilibrium concentrations were measured at wavelength λ = 530 nm (neutral red).

The amount of dye adsorbed in equilibrium, q$_{eq}$ (mg.g^{-1}) was calculated using Eq. (1) (Kharrazi et al., 2020):

$$q_{eq} = \frac{(C_0 - C_e) \times V}{m} \tag{1}$$

In which: C$_0$ (mg.L^{-1}) is the initial dye concentration; Ce (mg.L^{-1}) is the dye concentration in equilibrium; V (L) is the solution volume; and m (g) is the adsorbent mass (film).

2.5.1. Adsorption kinetics

The adsorption kinetics of the films were studied to determine the time required to achieve equilibrium, in addition to the adsorbed amount of neutral red dye (NR) at neutral pH and room temperature.

Thus, 0.1 g of the films were added in 10 mL of neutral red solutions at concentrations of 300 mg.L^{-1} for each film, which were inserted into amber bottles and kept under agitation at 100 rpm in agitating plate for 24 h. Then, aliquots of the 100 μL solutions were removed at predetermined intervals of 0; 10; 20; 30; 40; 50; 60; 180; 360; 1440 min, and their concentrations measured using UV-Visible spectroscopy (Applied Biosystems, model SP-2000 UV) at the wavelength λ = 530 nm (neutral red) in a spot absorbance analysis. The amount of dye adsorbed in equilibrium q$_{eq}$ (mg.g^{-1}) was also calculated using Eq. (1).

The removal efficiency of neutral red dye was calculated according to the equation below:

$$\text{Efficiency } (\%) = \frac{100 \times (C_0 - C_e)}{C_0} \tag{2}$$

In which: C$_0$ (mg.L^{-1}) is the initial concentration of solutions; C$_e$ (mg.L^{-1}) is the final concentration after a certain reaction time.

2.6. Data analysis

Data of the elemental chemical composition of the precursors was installed according to a completely randomized design with two treatments (residue and chitosan), in three repetitions, totaling six sample units. Data of the elemental chemical composition of the films was installed according to a completely randomized design with five treatments (T1, T2, T3, T4 and T5), in three repetitions, totaling fifteen sample units. Data were submitted to the analysis of variance (ANOVA) and the means were compared with each other by the Tukey's test at 95% probability when a significant effect of the treatments was observed.

Data of the neutral red adsorption isotherms of the films were fit according to the Langmuir and Freundlich models. The adsorption kinetics data of the films were fit to the pseudo-first order and pseudo-

second order models. The parameters were obtained and fitted in the SigmaPlot 11.0 software program.

3. Results and discussions

3.1. Chemical properties of precursors

Table 1 shows mean values of the elemental chemical composition of residue and chitosan. The analysis of variance indicated that there was a difference in elemental composition between residue and chitosan for the carbon, nitrogen, sulfur, oxygen and ash contents.

It was observed that the residue has favorable characteristics for activated carbon production, such as high carbon content and low ash content (1.75 %).

It is observed that the residue has a higher carbon content when compared to commercial chitosan. However, it also has a higher ash content, because it is residue from the furniture industry, where they use urea-based formaldehyde adhesives, as well as paints for making and finishing wood panels, and therefore they have higher inorganic content in their composition.

The type of raw material used to produce activated carbon and its manufacturing process greatly influence the ash content. The lower the inorganic content present in the AC, the better the adsorption process, since the mineral materials preferentially interact with water due to the hydrophilic character. Thus, the lower the ash content, the higher the adsorption capacity (Catelan and Mendes, 2019).

The high nitrogen content of commercial chitosan comes from the amine groups present in its structure. In obtaining chitosan via chitin deacetylation, the acetamide (–NHCOCH$_3$) groups of the remaining *N-acetylglucosamine* units of the precursor are converted into amino (–NH$_2$) groups at varying rates to originate the heteropolysaccharide with varying degrees of deacetylation (GD). Chitin is generally only considered chitosan when the GD becomes equal to or greater than 60%, being a percentage from which the biopolymer becomes soluble in dilute acid solutions (Alves and Mano, 2008).

Chitosan has a higher sulfur and oxygen content when compared to furniture industry residue. The biopolymer is composed of structural units of 2-amino-2-deoxy-D-glucopyranose and 2-acetamido-2-deoxy-D-glucopyranose joined by glycosidic bonds of type β (1→4) and has several OH groups in its composition (Karaer and Kaya, 2016).

3.2. Chemical properties of films

Table 2 shows the mean values of the elemental chemical composition of the AC and chitosan composite films and the pure chitosan film (T1). The analysis of variance indicated that there was a difference in the elemental composition of the films for the carbon, hydrogen, nitrogen, oxygen and ash contents.

The chitosan film (T1) has lower carbon and ash content when compared to the others. On the other hand, activated carbon and chitosan composite films have lower hydrogen, nitrogen and oxygen content when compared to the pure chitosan film. This change in the elemental

Table 1. Structural and elemental chemical composition of precursors.

Elemental composition (%)	*Pinus* spp. plywood panel residue	Chitosan
C	52.80 A	44.00 B
H	5.86 B	5.92 B
N	0.27 B	7.48 A
S	0.08 B	1.92 A
O	39.24 B	40.40 A
Ash	1.75 A	0.28 B

Means followed by the same capital letter between lines do not differ from each other at 5% significance by the Tukey's test.

Table 2. Elemental chemical composition of films.

Films	Percentage (%)				
	C	H	N	O	Ash
T1	45.15c	5.96a	7.75a	40.05a	0.02b
T2	56.65b	4.85b	5.09c	31.50b	1.28a
T3	56.60b	4.83b	5.38bc	31.20b	1.30a
T4	57.45a	4.38b	5.16bc	30.00c	1.34a
T5	57.35a	4.40b	5.45b	31.15b	1.38a

Means followed by the same lowercase letter between columns do not differ from each other at 5% significance by the Tukey's test. T1: chitosan; T2: activated carbon produced at 600 °C for 1 h + chitosan; T3: activated carbon produced at 600 °C for 2 h + chitosan; T4: activated carbon produced at 750 °C for 1 h + chitosan; T5: activated carbon produced at 750 °C for 2 h + chitosan.

composition of the films is generated by the composition of the activated carbon produced at different activation times and temperatures.

There was an increase in the carbon content of composite films as the carbon activation temperature increased. The T4 and T5 films have higher carbon content when compared to the others.

A carbon-rich product is formed during the carbonization process and subsequent activation of biomass due to the elimination of non-carbonaceous elements such as hydrogen, oxygen and nitrogen. This occurs due to partial degradation of organic matter and release of volatile substances (Pena et al., 2020). For example, the reduced hydrogen and oxygen content in activated carbon can be attributed to the loss of OH groups caused by dehydration, dehydrogenation reactions and disruption of hydrogen bonds in the charcoal structure (You et al., 2017). Therefore, the higher the activation temperature, the higher the carbon content and the lower hydrogen, oxygen and nitrogen contents.

The ash content in composite films is related to the presence of inorganic materials in the activated carbons, and it is observed that there was no significant difference between them. Organic matter degradation occurs during the charcoal activation process, with partial degradation of the carbonaceous matrix due to the volatilization of the carbon-rich compounds and the concentration of inorganic compounds which are difficult products to degrade (Jeong et al., 2016).
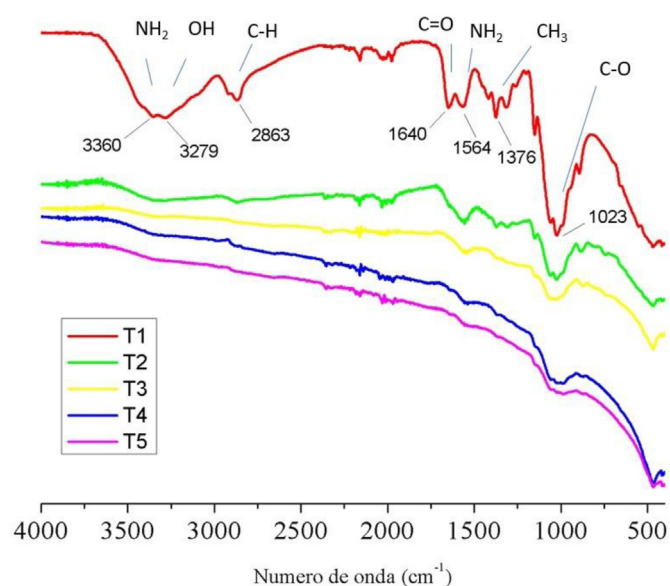
Figure 2. FTIR spectra of films. T1: chitosan; T2: activated carbon produced at 600 °C for 1 h + chitosan; T3: activated carbon produced at 600 °C for 2 h + chitosan; T4: activated carbon produced at 750 °C for 1 h + chitosan; T5: activated carbon produced at 750 °C for 2 h + chitosan.

3.3. Vibrational spectroscopy in the infrared region of films (FTIR)

Figure 2 shows the spectra of AC and chitosan composite and pure chitosan films. The functional groups present in the films can be interpreted from the absorption bands obtained in the analysis of electronic spectroscopy in the infrared region.

In the pure chitosan spectrum, the band close to 3360 and 3279 cm^{-1} refers to the binding stretch of the NH$_2$ group and the OH functional group, respectively (Marques Neto et al., 2019). It was observed that these bands are more intense in the T2 film when compared to other composite films, indicating the presence of hydroxylated structures in greater quantity.

The band close to 2863 cm^{-1} refers to the C–H binding stretch of the CH$_2$ group of pyranoses (Marques Neto et al., 2019). It was also observed that this band is slightly larger in the T2 film when compared to other composite films.

The characteristic bands of the biopolymer chitosan (T1) are observed in the region between 1700 and 1300. The band close to 1640 cm^{-1} is attributed to the axial deformation of C=O of the carbonyl, of the acetamide group, which corresponds to the acetylated part of the chitosan. The band close to 1564 cm^{-1} refers to the angular deformation of NH$_2$ and the band close to 1376 cm^{-1} is attributed to the angular deformation of C–H of the CH$_3$ group (Leucena et al., 2013). It is observed that these bands were reduced in the activated carbon and chitosan composite films.

The band close to 1023 cm^{-1} refers to the C–O binding stretching (Cho et al., 2012), and it is noted that this band is more intense in the T2 and T3 films when compared to the other composite films. The spectra of chitosan films containing activated carbon had similar bands to that of pure chitosan, however a strong effect is observed in the reduction of band intensities as temperature and activation time of charcoal added to the films are increased.

Activated carbons not only have carbon in their structure, but also some heteroatoms such as hydrogen, oxygen and nitrogen (Rahmi and Rizki, 2018). The increase in activation time and temperature promoted the reduction of surface groups in the carbonaceous structure (Montané et al., 2009), consequently indicating a reduction of bands in the spectra of activated carbon and chitosan composite films. As the activation temperature increases, the activated carbon structure becomes more aromatic, the higher the absorption of infrared radiation by the material, and as a consequence, the lower the reflectance, generating less intense bands in the spectrum. A higher ash concentration can still occur at a temperature equal to or higher than 750 °C, which can cover the chitosan structure and make it impossible to observe the characteristic bands of the polymer.

The band at 1564 cm^{-1} reduced the intensity and shifted between 1555 to 1533 cm^{-1} in the spectra of composite films, confirming the interaction between functional chitosan and activated carbon groups. However, band disappearance and a decrease in intensity is mainly related to covering chitosan with activated carbon and also with the ash present in treatments with higher temperatures and activation time.

Even to a lesser extent, the main chemical groups found in activated carbon and chitosan films are hydroxyl and amides, considered cationic exchangers, resulting in films with acidic characteristics. The electric charge, which surface groups can acquire when in solution, is able to favor the adsorption of the target molecule if it has an opposite charge (Shen et al., 2018).

3.4. X-ray diffraction spectroscopic analysis of films

Figure 3 shows the diffractograms obtained at 2θ from 10 to 50° for the activated carbon and chitosan composite and pure chitosan films. The characteristic peak for chitosan was observed around 2θ = 19.84° with high intensity, referring to the amorphous structure of the material.

The peak observed in the chitosan film diffractogram (T1) characterizes it as a semicrystalline material. This semicrystalline profile is
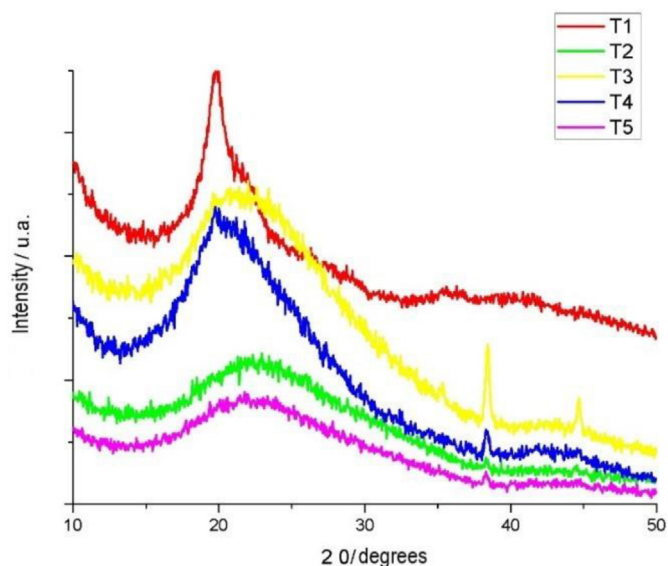
Figure 3. X-ray diffraction patterns of films. T1: chitosan; T2: activated carbon produced at 600 °C for 1 h + chitosan; T3: activated carbon produced at 600 °C for 2 h + chitosan; T4: activated carbon produced at 750 °C for 1 h + chitosan; T5: activated carbon produced at 750 °C for 2 h + chitosan.

related to the strong intramolecular and intermolecular interactions which provide this organization to the chitosan structure, characterized by hydrogen bonds formed between amine, amide, alcohol and other functional groups present in its structure (Gao et al., 2014).

The wide peak between 19° to 22° in AC and chitosan composite films is probably due to the peak overlap referring to the structure of chitosan (19.8°) and AC graphite (22°). The peaks at 22 and 44° correspond to the graphite lattice planes (002) and (100), respectively, and are typical of amorphous carbon (Yu et al., 2014).

Peaks in the AC and chitosan composite films were formed close to 38 and 44° when compared to the T1 film. The peak near 38° probably refers to some metal oxide because there was an increase in the inorganic content in the films with the increase in charcoal activation temperature (Table 2). The peak near 44° refers to the graphite structure of the AC present in the films.

3.5. Specific surface area and pore diameter of films

The isotherm shows the relationship between the molar amount of gas adsorbed or desorbed by a solid, the constant temperature, as a function of the gas pressure. The adsorption and desorption isotherms from N_2 to 77 K of activated carbon films with chitosan and pure chitosan are shown in Figure 4.

The T1 film adsorbed a lower volume of N_2 when compared to the other films. Among the composite films, it was noted that there was an
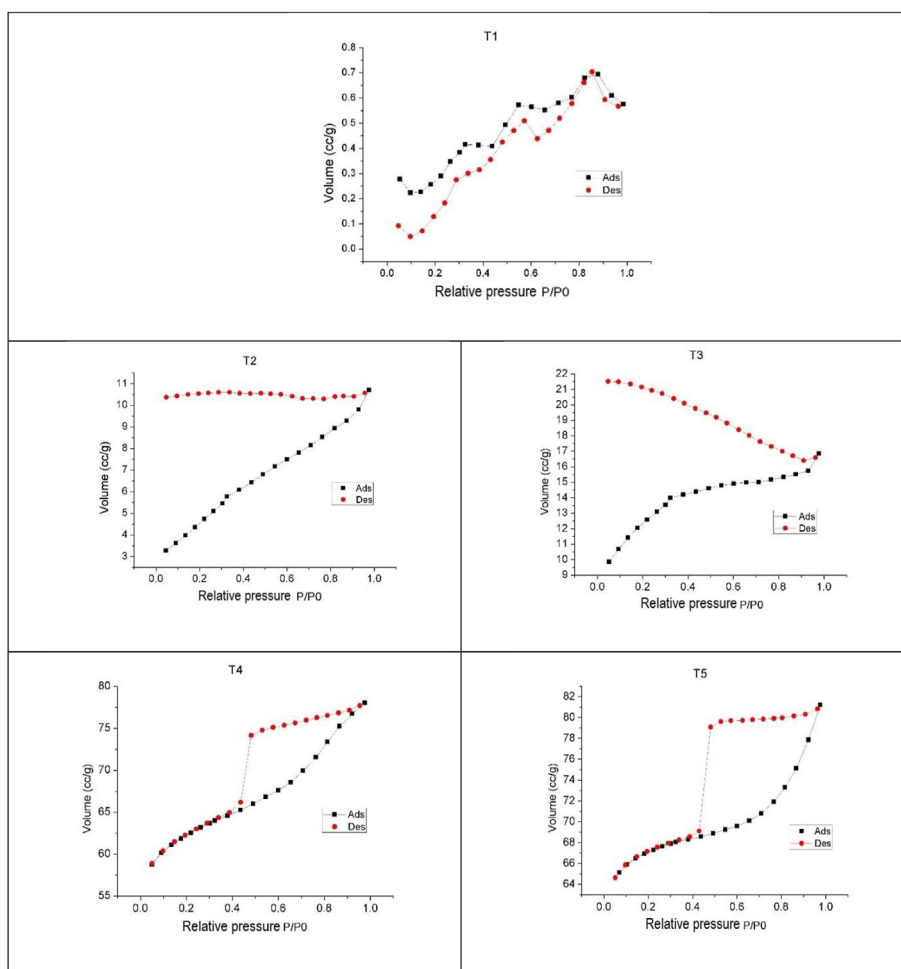
Figure 4. Adsorption and desorption isotherms of films. T1: chitosan; T2: activated carbon produced at 600 °C for 1 h + chitosan; T3: activated carbon produced at 600 °C for 2 h + chitosan; T4: activated carbon produced at 750 °C for 1 h + chitosan; T5: activated carbon produced at 750 °C for 2 h + chitosan.

increase in the volume of adsorbed N_2 as the time and temperature of charcoal activation increased.

According to Teixeira et al. (2001), the type VI isotherm is obtained from the gas adsorption by a low porous solid, with irregular porosity and an almost uniform surface, which occurs in pure chitosan films.

The isotherm of T2 and T3 films had similar behavior, with an opening between the adsorption and desorption curve. Such an opening occurs when there is incomplete combustion during carbonization and or activation of the precursor, resulting in retraction of the pores. In addition, there is low adsorption at low relative pressure which increases with increasing pressure (Dassanayake et al., 2018).

Adsorption and desorption curves do not approach at a relatively low pressure due to swelling of the porous structure of non-rigid charcoal, irreversible uptake of molecules in the pores, or in some cases by irreversible chemical interactions between adsorbate and adsorbent (Ye et al., 2019).

When gas condensation occurs inside the pores where the forces of attraction are greater due to the proximity between molecules, the condensation can occur at pressures lower than in non-porous solids. However, evaporation is hampered by the shape of the pores which are interconnected, and the adsorbed molecules can choose different paths of lower energy to travel during the adsorption. The different pathways characterize the hysteresis between the adsorption and desorption processes, and will be more pronounced the greater the pore size dispersion (Teixeira et al., 2001).

It is observed that the isotherms of the T4 and T5 films exhibit the usual form of type IV with hysteresis loop, indicating the presence of mesopores and micropores (Loya-González et al., 2019). Hysteresis is generally related to mesopores which appear to be produced by capillary evaporation of the condensed gas during the desorption process (Jung and Kim, 2014).

Table 3 shows the average values of surface area volume and pore diameter of composite and pure chitosan films. It is found that the presence of activated carbons and their activation processes modified the porous structure of the films. There was an increase in the surface area and pore volume of the films as the activation time and temperature of ACs increased.

Activated carbon serves as a support for the chitosan film, improving its mechanical, physical and chemical properties. The T5 film has a surface area 21 times larger when compared to T1. Sharififard et al. (2018) produced activated carbon and chitosan composite films for metal removal and found an increase in surface area of up to 38 times when compared to pure chitosan film.

The average pore diameter of composite films was around 1.85 nm, and lower than the chitosan film pores (T1), indicating that the presence of microporous charcoal alters film characteristics.

The carbonaceous matrix in reducing atmosphere at high activation temperatures undergoes several reforming reactions throughout the process, leading to partial gasification of charcoal and organic matter volatilization, in turn developing the porous structure and increasing its specific surface area (Palláres et al., 2018).

Table 3. Average surface area, volume and pore diameter values of films.

Films	Surface area (BET) – m²/g	Pore volume (cm³/g)	Pore diameter (nm)
T1	11.5	0.0018	2.26
T2	70.6	0.0160	1.83
T3	173.1	0.0200	1.84
T4	200.7	0.1080	1.88
T5	253.3	0.2030	1.89

T1: chitosan; T2: activated carbon produced at 600 °C for 1 h + chitosan; T3: activated carbon produced at 600 °C for 2 h + chitosan; T4: activated carbon produced at 750 °C for 1 h + chitosan; T5: activated carbon produced at 750 °C for 2 h + chitosan.

In addition to the temperature and time, the type of precursor, gas flow and type of activating agent play an important role in developing the porous structure and surface area of the charcoal during the activation process. The reaction speed varies between types of gases, as water vapor (for example) is more reactive and can promote activated carbons with greater surface area when compared to CO_2 due to the water molecule suffering greater diffusion into the carbon structure (Nor et al., 2013).

Reactions between charcoal and steam and between charcoal and CO_2 occur at distinct active sites when using the combination of steam and CO_2 during activation. Carbon dioxide forms new pores and elongates existing ones without significant change in width, while water vapor can increase the pore diameter (Coetzee el al., 2017).

3.6. Adsorption film isotherms

The adsorption isotherms of neutral red dye fit to the Langmuir and Freundlich models for activated carbon and chitosan composite and pure chitosan films are shown in Figure 5. Isotherms correlate the amount of the dye adsorbed per unit mass of the adsorbent (q_{eq}) with the concentration of neutral red in the adsorption equilibrium (C_{eq}).

It is observed that composite films adsorbed greater amount of dye when compared to T1 film (16 mg g^{-1}). There was an increase in the amount of dye adsorbed among the composite films with the increase in the activation time and temperature of activated carbons, reaching maximum adsorption of approximately 30 mg g^{-1}, referring to film T5. It should be noted that higher q values and lower C_{eq} values reflects in less quantity of the dye in solution and greater adsorption.

The adsorption parameters after fitting in the Freundlich and Langmuir models are presented in Table 4. It was found that the T1 film obtained better fit to the Langmuir model, while the others fit better to the Freundlich model, according to the R^2 value.

The Freundlich model considers the adsorbent consisting of multiple layers and is applicable for reversible adsorption on heterogeneous surfaces, with available sites with different adsorption energies. The Lagmuir model is mainly applicable to the homogeneous adsorption surface in monolayer, and therefore adsorption occurs without any interaction between the adsorbed molecules (Dahri et al., 2014).

The maximum adsorption capacity value is represented by the parameters q_0 and Kf of the Langmuir and Freundlich equation, respectively, and depend on factors such as the adsorbent characteristics and mass, as well as the adsorbate volume and concentration (Guerrero-Coronilla et al., 2015).

The nf parameter of the Freundlich equation is used to qualitatively verify the adsorption intensity, indicating the affinity of the adsorbent with respect to the neutral red dye and indicates favorable adsorption when it has values between 1 and 10 (Jawad et al., 2018).

All activated carbon and chitosan composite films showed favorable adsorption and T5 exhibited higher nf value, indicating higher adsorption intensity. A higher Kf value is also observed for this film, indicating greater adsorption capacity when compared to the others. These results can be explained by the fact that the AC present in the film has a larger surface area and larger pore volume, as indicated in Table 3.

The presence of activated carbon in the T5 film increased its adsorption capacity of the neutral red dye by approximately 87% when compared to the T1 film.

3.7. Adsorption kinetics of films

The adsorption kinetic curves fit to the pseudo-first order and pseudo-second order models of activated carbon and chitosan
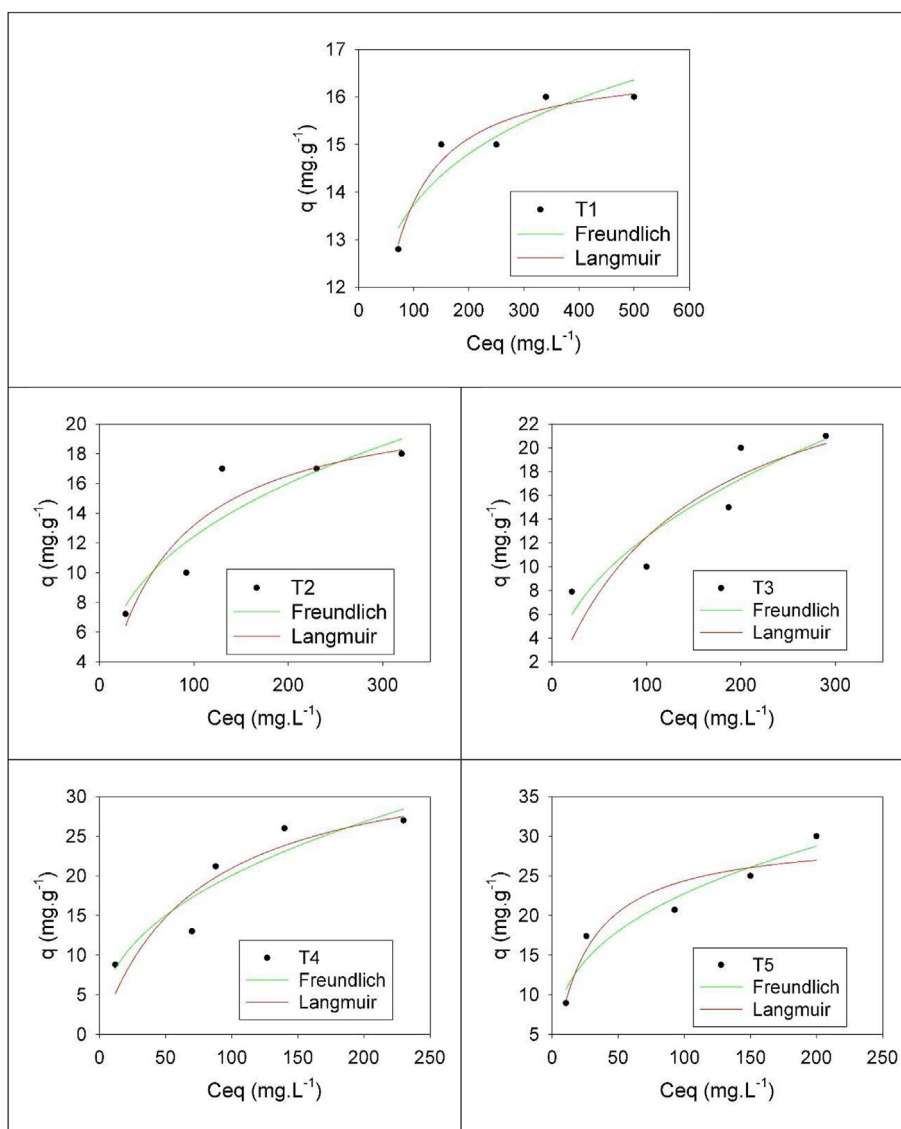
Figure 5. Adsorption isotherms of the neutral red dye of the films in different concentrations. T1: chitosan; T2: activated carbon produced at 600 °C for 1 h + chitosan; T3: activated carbon produced at 600 °C for 2 h + chitosan; T4: activated carbon produced at 750 °C for 1 h + chitosan; T5: activated carbon produced at 750 °C for 2 h + chitosan.

composite films and pure chitosan film are shown in Figure 6. The amount of adsorbed neutral red dye (q) are correlated with the time (min) in the kinetic study graphs. It is observed that composite films adsorbed a greater amount of neutral red dye when compared to pure chitosan film (T1). Regardless of the film, it is observed that the adsorption rate increases rapidly in the first 10 min due to the occupation of free active sites and then tends to decrease with the passage of time.

Only the T2 film came into equilibrium in 24 h when compared to the others. This means that other films may still have active sites available and require more reaction time to reach equilibrium. The reaction speed is fast at first and ceases or slows down over time due to lower availability of active sites and functional groups (Sethy et al., 2019).

The adsorption kinetic parameters obtained after fitting the pseudo-first order and pseudo-second order models and their determination coefficients are presented in Table 5.

Table 4. Freundlich and Langmuir parameters for adsorption of neutral red dye from composite and pure chitosan films.

Films	Freundlich			Langmuir		
	Kf	nf	R^2	q0	b	R^2
T1	8.31	9.09	0.87	16.75	0.04	0.94
T2	1.32	2.70	0.88	22.13	0.01	0.85
T3	1.41	2.11	0.85	30.51	0.01	0.76
T4	2.90	2.38	0.86	36.20	0.01	0.83
T5	4.83	3.03	0.93	30.21	0.04	0.91

Kf = Freundlich experimental constant; nf = constant indicating adsorption intensity; q0 = maximum monolayer coverage capacity (mg.(g-1), b = Langmuir constant (L.mg-1)); R_2 = Coefficient of determination; T1: chitosan; T2: activated carbon produced at 600 °C for 1 h + chitosan; T3: activated carbon produced at 600 °C for 2 h + chitosan; T4: activated carbon produced at 750 °C for 1 h + chitosan; T5: activated carbon produced at 750 °C for 2 h + chitosan.
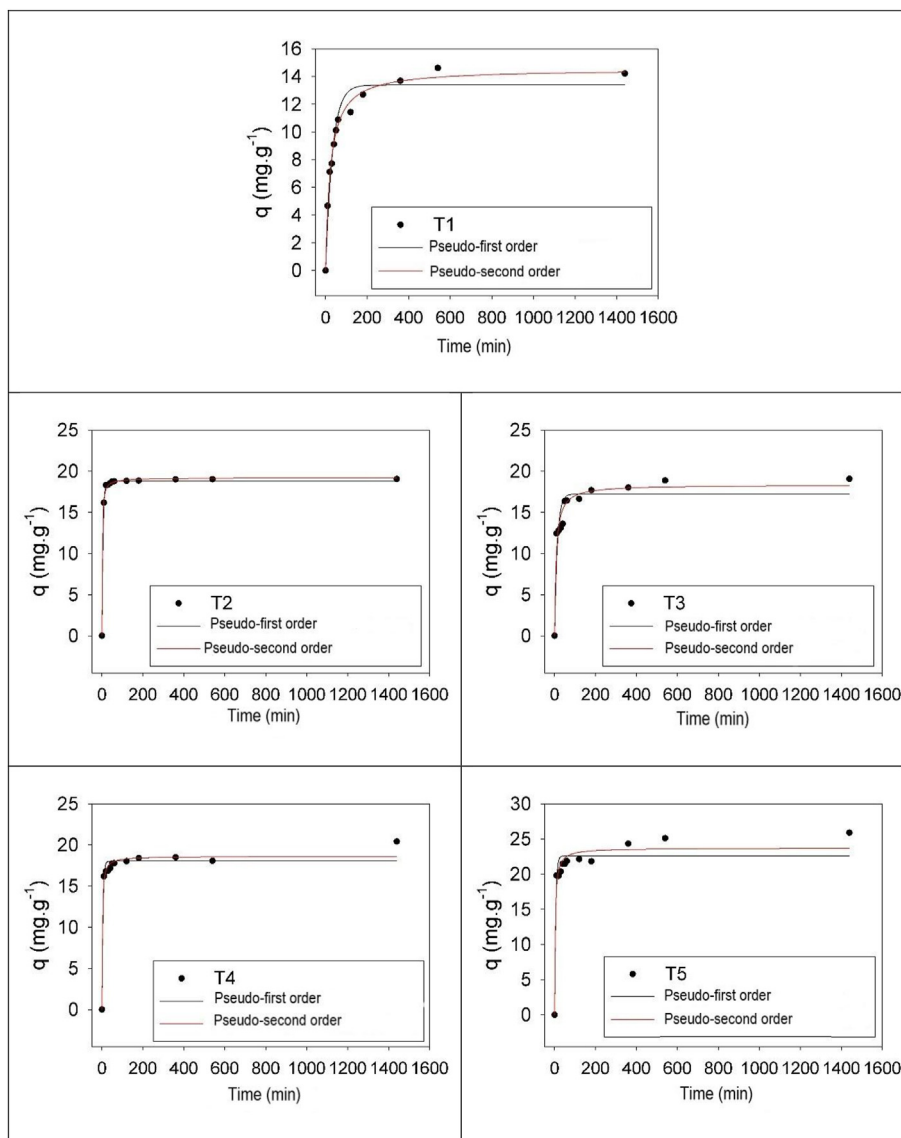
Figure 6. Adsorption kinetic curves of the neutral red dye of the films. T1: chitosan; T2: activated carbon produced at 600 °C for 1 h + chitosan; T3: activated carbon produced at 600 °C for 2 h + chitosan; T4: activated carbon produced at 750 °C for 1 h + chitosan; T5: activated carbon produced at 750 °C for 2 h + chitosan.

Table 5. Parameters of pseudo-first order and pseudo-second order kinetic curves of composite and pure chitosan films.

Films	Pseudo-first order			Pseudo-second order			Qcal
	q	K_1	R^2	q	K_2	R^2	
T1	18.80	0.19	0.98	19.185	0.033	0.99	14.22
T2	17.22	0.07	0.89	18.33	0.007	0.96	19.05
T3	18.03	0.21	0.97	18.60	0.027	0.98	19.06
T4	18.08	0.21	0.97	18.69	0.025	0.99	20.41
T5	13.38	0.03	0.96	15.243	0.002	0.99	25.89

q = adsorbed quantity per gram of adsorbent in equilibrium (mg.g^{-1}); k_1 = constant of the adsorption rate of pseudo-first order (g.mg^{-1}.min^{-1}); k_2 = constant of the adsorption rate of pseudo-second order (g.mg^{-1}.min^{-1}); R^2 = coefficient of determination; qcal = calculated quantity of the adsorbed dye per gram of the adsorbent (mg.g^{-1}); T1: chitosan; T2: activated carbon produced at 600 °C for 1 h + chitosan; T3: activated carbon produced at 600 °C for 2 h + chitosan; T4: activated carbon produced at 750 °C for 1 h + chitosan; T5: activated carbon produced at 750 °C for 2 h + chitosan.

According to the coefficient of determination (R^2) and qcal values, all adsorbent materials produced had better fits associated with the pseudo-second order model.

Higher adsorption capacity (q) was found for the T5 film and lower adsorption of the T1 film. This result was already expected due to the larger pore volume and larger surface area of the AC produced at higher temperature and longer activation time when compared to the others.

The mean removal efficiency values of neutral red dye are presented in Table 6. It is observed that all chitosan with activated carbon composite films have higher efficiency when compared to T1 film, which only obtained 49.33%.

It is observed that the T2 film stabilizes in about 360 min of reaction, indicating that it has entered equilibrium and there are no more sites available for adsorption, while the other films need more reaction time to stabilize.

It was found that there was not much difference between the maximum neutral red dye removal efficiency for the T2 and T3 composite films in 24 h of reaction, around 63.5%.

Between the T4 and T5 films, it was observed that there was an increase in the dye removal efficiency as the AC production time was

Table 6. Neutral red dye removal efficiencies from activated carbon and chitosan composite and pure chitosan films.

Efficiency (%)					
Time (min)	T1	T2	T3	T4	T5
10	15.57	54.00	41.44	53.96	66.03
20	23.73	61.03	42.58	56.03	65.80
30	25.75	61.20	43.62	56.26	67.93
40	30.40	61.78	45.34	57.18	71.55
50	33.73	62.47	54.54	59.14	71.55
60	36.32	62.58	54.77	59.25	72.90
120	38.10	62.76	55.46	60.06	73.79
180	42.35	62.87	58.96	61.38	72.76
360	45.73	63.39	60.05	61.66	81.09
560	48.73	63.45	62.93	61.95	83.68
1440	49.33	63.50	63.56	68.04	86.32

T1: chitosan; T2: activated carbon produced at 600 °C for 1 h + chitosan; T3: activated carbon produced at 600 °C for 2 h + chitosan; T4: activated carbon produced at 750 °C for 1 h + chitosan; T5: activated carbon produced at 750 °C for 2 h + chitosan.

increased. The T5 film obtained greater removal efficiency (86%) of the dye in 24 h when compared to the others, and efficiency of 66% in just 10 min of reaction.

The presence of activated carbon in the T5 film increased its neutral red dye removal efficiency by approximately 43% when compared to the T1 film. The higher removal efficiency of neutral red dye by T5 film is related to the larger surface area and larger pore volume, as indicated in Table 3.

4. Conclusions

The *Pinus* spp. plywood panel residue has favorable chemical characteristics for producing activated carbon, such as high carbon content and low ash content, and the activation process using a combination of gases such as water vapor and CO_2 was effective in producing microporous activated carbons.

The presence of activated carbons in the films provided improvements in physical properties such as increased surface area and pore volume, and consequently greater adsorption capacity of the neutral red dye, verifying synergistic effect on adsorption.

The T5 film has higher adsorption capacity and neutral red dye removal when compared to the other films, with 30 mg g^{-1} and 86% in 24 h, respectively.

Declarations

Author contribution statement

Fabiana Paiva de Freitas: Conceived and designed the experiments; Performed the experiments; Analyzed and interpreted the data; Wrote the paper.

Ana Márcia Macedo Ladeira Carvalho, Angélica de Cássia Carneiro Oliveira: Analyzed and interpreted the data.

Mateus Alves de Magalhães, Mariana Fonseca Xisto: Performed the experiments; Contributed reagents, materials, analysis tools or data.

Wagner Davel Canal: Contributed reagents, materials, analysis tools or data.

Data availability statement

Data included in article/supp. material/referenced in article.

Declaration of interests statement

The authors declare no conflict of interest.

Additional information

No additional information is available for this paper.

References

Alves, N.M., Mano, J.F., 2008. Chitosan derivatives obtained by chemical modifications for biomedical and environmental applications. Int. J. Biol. Macromol. 43 (5), 401–414.

Andrade, S.M.B., Rocha, B.G., Belermino, D.D., Galvão, A.O., 2012. Preparação e caracterização de membranas de quitosana de camarões (Litopenaeus Vannamei) e caranguejos (Ucides Cordatus). Revista de biologia, farmácia e manejo agrícola, pp. 102–111.

Associação Brasileira de Normas Técnicas, 1986. NBR 8112: Carvão Vegetal: Análise Imediata. Rio de Janeiro, p. 8.

Carvalho, V.L., Gonçalves, J.O., Silva, A., Cadaval Junior, T.R., Pinto, L.A.A., Lopes, T.J., 2019. Separation of anthocyanins extracted from red cabbage by adsorption onto chitosan films. Int. J. Biol. Macromol. 131, 905–911.

Catelan, T.C., Mendes, A.N.F., 2019. Produção de carvão ativado a partir da palha de milho e posterior utilização para remoção do corante azul de metileno de efluentes aquosos. Brazilian J. Product. Eng. 5 (3), 139–154.

Cho, D.-W., Jeon, B.-H., Chon, C.-M., Kim, Y., Schwartz, F.W., Lee, E.-S., Song, H., 2012. A novel chitosan/clay/magnetite composite for adsorption of Cu(II) and As(V). Chem. Eng. J. 200 – 202, 654–662.

Coetzee, G.H., Sakurovs, R., Neomagus, H.W.J.P., Everson, R.C., Mathews, J.P., Bunt, J.R., 2017. Particle size influence on the pore development of nanopores in coal gasification chars: from micron to millimeter particles. Carbon N. Y. 112, 37–46.

Dahri, M.K., Kooh, M.R.R., Lim, L.B.L., 2014. Water remediation using low cost adsorbent walnut shell for removal of malachite green: equilibrium, kinetics thermodynamic and regeneration studies. J. Environ. Chem. Eng. 2 (3), 1434–1444.

Dassanayake, R.S., Gunathilake, C., Abidi, N., Jaroniec, M., 2018. Activated carbon derived from chitin aerogels: preparation and CO_2 adsorption. Cellulose 25 (3), 1911–1920.

DIN EN 15104, 2011a. Determination of Total Content of Carbon, Hydrogen and Nitrogen – Instrumental Methods. Berlim: CEN, p. 15.

DIN EN 15296, 2011b. Conversion of Analytical Results from One Basis to Another. Berlim: CEN, p. 15.

Gao, Q., Zhu, H., Luo, W.-J., Wang, S., Zhou, C.-G., 2014. Preparation, characterization, and adsorption evaluation of chitosan-functionalized mesoporous composites. Microporous Mesoporous Mater. 193, 15–26.

Guerrero-Coronilla, I., Morales-Barrera, L., Cristiani-Urbina, E., 2015. Kinetic, isotherm and thermodynamic studies of amaranth dye biosorption from aqueous solution onto water hyacinth leaves. J. Environ. Manag. 152, 99–108.

Gupta, V.K., Pathania, D., Sharma, S., Agarwal, S., Singh, P., 2013. Remediation and recovery of methyl orange from aqueous solution onto acrylic acid grafted *Ficus carica* fiber: isotherms, kinetics and thermodynamics. J. Mol. Liq. 177, 325–334.

Iram, M., Guo, C., Guan, Y., Ishfaq, A., Liu, H., 2010. Adsorption and magnetic removal of neutral red dye from aqueous solution using Fe$_3$O$_4$ hollow nanospheres. J. Hazard Mater. 181, 1039–1050.

Jawad, A.H., Norrahma, S.S.A., Hameed, B.H., Ismail, K., 2018. Chitosan-glyoxal film as a superior adsorbent for two structurally different reactive and acid dyes: adsorption and mechanism study. Int. J. Biol. Macromol. 135, 569–581.

Jeong, C.Y., Dodla, S.K., Wang, J.J., 2016. Fundamental and molecular composition characteristics of biochars produced from sugarcane and rice crop residues and by-products. Chemosphere 142 (4).

Jung, S., Kim, J., 2014. Production of biochars by intermediate pyrolysis and activatedcarbons from oak by three activation methods using CO_2. J. Anal. Appl. Pyrol. 107, 116–122.

Karaer, H., Kaya, I., 2016. Synthesis, characterization of magnetic chitosan/active charcoal composite and using at the adsorption of methylene blue and reactive blue4. Microporous Mesoporous Mater. 232, 26–38.

Kharrazi, S.M., Mirghaffari, N., Dastgerdi, M.M., Soleimani, M., 2020. A novel post-modification of powdered activated carbon prepared from lignocellulosic waste through thermal tension treatment to enhance the porosity and heavy metals adsorption. Powder Technol. 366, 358–368.

Kumar, M., Xiong, X., Wan, Z., Sun, Y., Tsang, D.C.W., Gupta, J., Gao, B., Cao, X., Tang, J., Ok, Y.S., 2020. Ball milling as a mechanochemical technology for fabrication of novel bio- char nanomaterials. Bioresour. Technol. 312, 123613.

Leucena, G.L., Silva, A.G., Honório, L.M.C., Santos, V.D., 2013. Remoção de corantes têxteis a partir de soluções aquosas por quitosana modificada com tioacetamida. Revista Ambiente e Água 8 (1), 144–154.

Liu, W., Zhang, J., Zhang, C., Ren, L., 2012. Preparação e avaliação de adsorventes contendo ferro ativado a carvão para remoção aprimorada de Cr (VI): estudo de mecanismo. Chem. Eng. J. 189 (190), 295–302.

Loya-González, D., Loredo-Cancino, M., Soto-Regalado, E., Rivas-García, P., Cerino-Córdova, F.J., Garcia-Reyes, R.B., Bustos-Martínez, D., Estrada-Baltazar, A., 2019. Optimal activated carbon production from corn pericarp: a life cycle assessment approach. J. Clean. Prod. 219, 316–325.

Marques Neto, J.O., Belato, C.R., Silva, D.C., 2019. Iron oxide/carbon nanotubes/chitosan magnetic composite film for chromium species removal. Chemosphere 218, 391–401. https://www.sciencedirect.com/science/article/abs/pii/S0032591020300772.

Montané, D., Fierro, V., Marêché, J., Aranda, L., Celzard, A., 2009. Activation of biomass-derived charcoal with supercritical water. Microporous Mesoporous Mater. 119, 53–59.

Nor, N.M., Chung, L.L., Teong, L.K., Mohamed, A.R., 2013. Synthesis of activated carbon from lignocellulosic biomass and its applications in air pollution control—a review. J. Environ. Chem. Eng. 1, 658–666.

Palláres, J., González-Cencerrado, A., Arauzo, I., 2018. Production and characterization of activated carbon from barley straw by physical activation with carbon dioxide and steam. Biomass Bioenergy 115, 64–73.

Pena, J., Villot, A., Gerente, C., 2020. Pyrolysis chars and physically activated carbons prepared from buckwheat husks for catalytic purification of syngas. Biomass Bioenergy 132.

Rahmi, L., Rizki, N., 2018. Preparation of Polyethylene Glycol Diglycidyl Ether (PEDGE) crosslinked chitosan/activated carbon composite film for Cd2+ removal. Carbohydr. Polym. 199, 499–505.

Sethy, T.R., Pradhan, A.K., Sahoo, P.K., 2019. Simultaneous studies on kinetics, bio-adsorption behavior of chitosan grafted thin film nanohydrogel for removal of hazardous metal ion from water. Environ. Nanotechnol. Monit. Manag. 12.

Sharififard, H., Nabavinia, M., Soleimani, M., 2016. Evaluation of adsorption efficiency of activated carbon/chitosan composite for removal of Cr (VI) and Cd (II) from single and bi-solute dilute solution. Adv. Environ. Technol. 4, 215–227.

Sharififard, H., Shahraki, Z.H., Rezvanpanah, E., Rad, S.H., 2018. A novel natural chitosan/activated carbon/iron: bio-nanocomposite: sonochemical synthesis, characterization, and application for cadmium removal in batch and continuous adsorption process. Bioresour. Technol. 270, 562–569.

Shen, J., Huang, G., An, C., Xin, X., Huang, C., Rosendahl, S., 2018. Removal of Tetrabromobisphenol A by adsorption on pinecone-derived activated charcoals: synchrotron FTIR, kinetics and surface functionality analyses. Bioresour. Technol. 247, 812–820.

Teixeira, V.G., Coutinho, F.M.B., Gome, A., 2001. Principais métodos de caracterização da porosidade de resinas à base de Divinilbenzeno. Quím. Nova 24 (6), 808–818.

Tran, C.D., Duri, S., Delneri, A., Franko, M., 2013. Chitosan-cellulose composite materials: preparation, characterization and application for removal of microcystin. J. Hazard Mater. 252–253, 355–366.

Ye, J., Tao, S., Li, S., Tang, D., Wang, J., Xu, H., 2019. Abnormal adsorption and desorption of nitrogen at 77 K on coals: study of causes and improved experimental method. J. Nat. Gas Sci. Eng. 70, 29–40.

You, S., Ok, Y.S., Chen, S.S., Tsang, D.C.W., Kwon, E.E., Lee, J., Wang, ChH., 2017. A critical review on sustainable biochar system through gasification: energy and environmental applications. Bioresour. Technol. 246, 242–253.

Yu, J., Guo, M., Muhammad, F., Wang, A., Zhang, F., Lin, Q., Zhu, G., 2014. One-pot synthesis of highly ordered nitrogen-containing mesoporous carbon with resorcinol-urea-formaldehyde resin for CO_2 capture. Carbon N. Y. 69, 502–514.

Zhang, L., Luo, H., Liu, P., Fang, W., Geng, J., 2016. A novel modified graphene/oxide/chitosan composite used as an adsorbent for Cr (VI) in aqueous solutions. Int. J. Biol. Macromol. 87, 586–596.